Journal of Biomedical Materials Research Part B: Applied Biomaterials

Electrospun fibroin/polyurethane hybrid meshes: manufacturing, characterization and potentialities as substrates for haemodialysis arteriovenous grafts

Journal:	*Journal of Biomedical Materials Research: Part B - Applied Biomaterials*
Manuscript ID	JBMR-B-17-0812.R1
Wiley - Manuscript type:	Original Research Report
Date Submitted by the Author:	n/a
Complete List of Authors:	van Uden, Sebastião; Bioengineering Laboratories S.r.l. (BEL), R&D; Politecnico di Milano Dipartimento di Elettronica Informazione e Bioingegneria, Catto, Valentina; Bioengineering Laboratories S.r.l. (BEL), R&D Perotto, Giovanni; Istituto Italiano di Tecnologia, Smart Materials Athanassiou, Athanassia; Istituto Italiano di Tecnologia, Smart Materials Redaelli, Alberto; Politecnico di Milano Dipartimento di Elettronica Informazione e Bioingegneria Greco, Francesco; Bioengineering Laboratories S.r.l. (BEL), R&D Riboldi, Stefania; Bioengineering Laboratories S.r.l. (BEL), R&D
Keywords:	Hybrid, Semi-degradable material, Polyurethane fibroin blend, Electrospun vascular graft, Haemodialysis

Electrospun fibroin/polyurethane hybrid meshes: manufacturing, characterization and potentialities as substrates for haemodialysis arteriovenous grafts

Sebastião van Uden[1,2], Valentina Catto[1], Giovanni Perotto[3], Athanassia Athanassiou[3], Alberto C. L. Redaelli[2], Francesco G. Greco[1], Stefania A. Riboldi[1,*]

[1] Bioengineering Laboratories S.r.l., Cantù (CO), Italy

[2] Politecnico di Milano, Milan (MI), Italy

[3] Smart Materials, Istituto Italiano di Tecnologia, Via Morego, 30, Genova 16163, Italy

*Corresponding author:

Stefania A. Riboldi

Tel: +39.031-7377739

Fax: +39.031-730467

E-mail: sriboldi@bioengineeringlab.com

Address: Viale Cesare Cattaneo 20, Cantù (CO) 22063, Italy

Electrospun fibroin/polyurethane meshes: manufacturing, characterization and potentialities as substrates for haemodialysis arteriovenous grafts

Abstract: Several attempts made so far to combine silk fibroin and polyurethane, in order to prepare scaffolds encompassing the bioactivity of the former with the elasticity of the latter, suffer from critical drawbacks concerning industrial and clinical applicability (e.g., separation of phases upon processing, use of solvents unaddressed by the European Pharmacopoeia, use of degradable polyurethanes). Overcoming these limitations, in this study we report the successful blending of regenerated silk fibroin with a medical-grade, non-degradable polyurethane using formic acid and dichloromethane, and the manufacturing of hybrid, semi-degradable electrospun tubular meshes with different ratios of the two materials. Physicochemical analyses demonstrated the maintenance of the characteristic features of fibroin and polyurethane upon solubilisation, blending, electrospinning and post-processing with ethanol or methanol. Envisioning their possible application as semi-degradable substrates for haemodialysis arteriovenous grafts, tubular meshes were further characterized, showing sub-micrometric fibrous morphologies, tuneable mechanical properties, permeability before and after puncture in the same order of magnitude as commercial grafts currently used in the clinics. Results demonstrate the potential of this material for the development of hybrid, new-generation vascular grafts with disruptive potential in the field of *in situ* tissue engineering.

Keywords: hybrid, semi-degradable material, polyurethane fibroin blend, electrospun vascular graft, haemodialysis;

1. Introduction

In situ tissue engineering strategies, which rely on the patient's body as a bioreactor in alternative to *in vitro* culture before implantation, have been showing disruptive potential for clinical cardiovascular applications[(1)–(5)]. This approach, lately also called "endogenous tissue regeneration", proposes ready-to-use biodegradable scaffolds, with low manufacturing cost and lead time, designed to improve local tissue functionality while triggering regeneration. In this scenario, arteriovenous vascular grafts for haemodialysis represent a particularly interesting application of *in situ* tissue engineering, since these scaffolds could be used as "off-the-shelf" prostheses, offering the ultimate valuable and durable vascular access alternative for patients in the need for long-term haemodialysis, currently facing the choice between suboptimal alternatives, i.e. native fistulae or fully synthetic grafts[(6)]. In fact, if properly designed, biodegradable arteriovenous vascular grafts would allow for immediate puncturing after implantation (early cannulation), thus enabling urgent haemodialysis, and would progressively evolve into a healthy native vascular tissue, granting superior patency on the long term. However, considering the acellular character of this approach, the successful outcome relies exclusively on the scaffold's material. This requires extra material engineering focus on the development of scaffolds that possess the desired predictable dynamic response at short-, medium- and long-term after implantation.

In this direction, one promising strategy consists in combining a natural degradable material with a synthetic inert polymer, providing a "hybrid" alternative to the puristic *in situ* tissue engineering approach, which encompasses fully degradable scaffolds. Indeed, the implantation of a semi-degradable vascular graft would safeguard the mechanical functionality in the long-run, since the non-degradable material would remain inert *in situ*, while the natural material would be progressively replaced by newly developed tissue.

Silk fibroin and polyurethane are two possible candidates to pursue the "hybrid" goal**. Silk fibroin has been approved by the US Food and Drug Administration (FDA) to be used in the form of surgical suture**[7]**, it has demonstrated to induce a negligible inflammatory response**[8],[9]**, to possess good biocompatibility properties *in vitro* and *in vivo* (rats)**[10]**, and suitable hemocompatibility in a canine model**[11]**. Additionally, Zhang *et al.* demonstrated how ePTFE grafts (under commercialization for vascular access application), when coated internally with a layer of silk fibroin, increased their hemocompatibility in rabbits as a result of a natural development of a layer of endothelial cells, resembling the morphology of the intima layer in native blood vessels**[12]**. As regards polyurethanes, their overall biocompatibility properties are generally deemed to be good; however, as addressed in the following, the wide range of possible formulations might significantly influence their degree of biocompatibility**[13]**. The combination of polyurethane and silk fibroin** has already been proposed in different formulations, morphologies, and ratios[14]–[34] with the aim to prepare scaffolds encompassing the bioactive compatibility and degradability of fibroin together with the elasticity and long-term biostability of polyurethanes. Studies that report the coupling of these two materials, however, have one or more critical drawbacks concerning industrial and clinical applicability. The majority of these works use solvents unaddressed **or belonging to Class 1 (Solvents to be avoided)** in the European Pharmacopoeia[14]–[20],[35] (e.g. hexa-fluoro-isopropanol, also characterized by exorbitant costs, extreme volatility and difficult manageability), or polyurethanes that are degradable and/or not suitable for long-term medical application[18]–[28],[36], which would unlikely pass the exam of regulatory approval necessary for product certification and commercialization. Other works report the development of composite scaffolds[14],[15],[22],[29]–[32],[37], where fibroin and polyurethane are present in different, non-coalescent phases, and are therefore highly susceptible to separation and delamination[30],

especially upon post-processing treatments (such as crystallization and sterilization, known to induce different volumetric changes in the natural and in the synthetic phases) or during *in vivo* remodelling. Both Bai *et al.*[27] and Liu *et al.*[26] report effective electrospinning of a polyurethane solution containing dispersed fibroin particles. This strategy potentially succeeds in gathering the elastic properties of polyurethane with the biocompatibility of silk fibroin; however, upon electrospinning, the non-dissolved fibroin particles are trapped inside polyurethane fibres, possibly hindering the fibres' mechanical resistance and reducing surface exposure suitable for cell attachment, therefore hampering the bioactive potential of fibroin.

Iizuka et al.[34] developed an interesting method to blend fibroin and polyurethane using an organic solvent addressed by the European Pharmacopoeia. However, this strategy results in a blend with unknown concentrations of fibroin, possibly failing to achieve consistent results from different batches.

Herein, the development of a hybrid semi-degradable material made of fibroin and polyurethane is reported with the potential for *in situ* vascular tissue engineering applications, such as innovative arteriovenous vascular grafts for haemodialysis. Overcoming the limitations of the above cited studies, we processed a blend of regenerated silk fibroin with a **medical-grade**[38], non-degradable polyurethane to prepare electrospun semi-degradable hybrid tubular scaffolds with an extracellular matrix-*like* morphology. The proposed method makes use of a novel sustainable solvent system complying with the directions of the European Pharmacopoeia for the development of medical implants[35]. The effects produced on the raw materials by the solvent mixture, blending, electrospinning, and post-processing treatments were investigated in order to successfully maintain the intrinsic properties associated to fibroin and polyurethane. Moreover, the versatility of the proposed process was demonstrated, allowing for the manufacturing of meshes with tuneable concentrations of raw materials, which were characterized in terms of mechanical properties, morphology and

permeability. Finally, in anticipation of their possible application as substrates for arteriovenous vascular grafts, the permeability of the meshes after puncture was assessed.

2. Materials and Methods

2.1 Materials

Bombyx mori cocoons were provided by the Council of Research and Experiments in Agriculture, Apiculture and Sericulture Unit (CREA-API; Padua, Italy). Poly-carbonate-urethane (Carbothane® Aromatic, AC–4075A) pellets (PP, polyurethane pellets) were kindly supplied by Lubrizol (Wickliffe, OH, United States). All other chemical reagents were obtained from Carlo Erba (Cornaredo, Italy) unless otherwise mentioned.

2.2 Preparation of regenerated *Bombyx mori* silk fibroin

Bombyx mori cocoons were degummed at 120°C for 15 min and washed to extract the sericin. Extracted fibroin fibres were solubilized in a 9.3 M lithium bromide solution (T = 60 ± 2°C, t = 3h under shaking) to obtain a final concentration of 10% w/v fibroin. The solution was then diluted with warm deionized water to obtain a 2% w/v fibroin concentration, filtered and dialyzed for three days using cellulose membrane tubing (M_w cut-off = 14,000 Da) to eliminate lithium bromide salts. Finally, fibroin films (FF) were prepared by solvent casting. Please, refer to Table 1 for the complete list of the samples and acronyms used in this study.

2.3 Blending silk fibroin and polyurethane

The fibroin/polyurethane blend solution was prepared by first dissolving each raw material separately and later joining them into one solution. Briefly, fibroin films were cut into small pieces and dissolved (T = room temperature (RT), t = 1h, 150 rpm) in formic acid (FA). In parallel, polyurethane was dissolved (T = RT, t = 1h, 250 rpm) in a 1:2 ratio of FA and dichloromethane (DCM), respectively. The polyurethane solution was then progressively transferred into the fibroin solution and further stirred (T = RT, t = 15 min, 150 rpm) to

achieve a blend solution with a final concentration of 2% w/v of each material within a 3:2 ratio of FA and DCM, respectively.

The blend solution was either used to produce blend films by solvent casting (BFS), to evaluate the blending effect on the raw materials, or to prepare blend electrospun samples (ENC, electrospun non-crystallized), using the parameters described in Table 1, to assess potential damages induced by electrospinning. Moreover, in order to evaluate the effect of solvents on the single raw materials, control films of pure fibroin (FFS) and pure polyurethane (PFS) were prepared by casting solutions prepared as described above for the blend, but skipping the addition of polyurethane and fibroin, respectively.

Finally, with the aim of developing a more industrially-sustainable crystallization treatment for silk fibroin, as an alternative to the common practice with methanol, an ethanol-based process was tested. Ethanol-crystallized electrospun blend samples (EtOH) were prepared by post-treating ENC samples in a descending series of ethanol/demineralized water solutions, upon stirring at 150 rpm: 50% v/v (1h), 50% v/v (15h), 25% v/v (1h), 25% v/v (1h), 100% H_2O (1h). EtOH samples were used to evaluate the post-treatment effect on the raw materials, the development of β-sheet conformations and the removal efficiency of solvents. As a control, methanol-crystallized electrospun blend samples (MeOH) were prepared by dipping ENC samples in a solution of 80% v/v methanol/demineralized water for 10 minutes.

2.4 Electrospinning of hybrid tubular meshes

The feasibility of manufacturing hybrid electrospun tubular meshes with tuneable fibroin/polyurethane ratios was evaluated by processing the following different blend solutions: 1% w/v fibroin and 3% w/v polyurethane (SF25PU75), 2% w/v fibroin and 2% w/v polyurethane (SF50PU50), and 3% w/v fibroin and 1% w/v polyurethane (SF75PU25). The samples were electrospun using the same electrospinning parameters employed on the

preparation of samples ENC, EtOH and MeOH (Table 1). Briefly, the blend solution was loaded into a solvent resistant syringe controlled by a pump delivering a constant flow rate (2.5 mL/h) to a spinneret (+17 kV), which was moving (velocity = 5 mm/s; path length = 20 cm) in parallel to a rotating (1000 rpm) metal rod collector (diameter = 8 mm; L = 32 cm), covered with aluminium foil, over a total period of 8 hours for each formulation. Electrospun hybrid tubular meshes were post-treated using the same crystallization protocol described above to prepare EtOH samples.

2.5 Characterization

2.5.1 Physicochemical properties

Physicochemical analyses were made on samples PP, PFS, FF, FFS, BFS, ENC, EtOH and MeOH, by Fourier transform infrared (FTIR) spectroscopy (N=3) and differential scanning calorimetry (DSC), to evaluate the effects of solvent mixture, blending, electrospinning, and post-treatment on the raw materials. FTIR was performed using an attenuated total reflectance spectrometer, acquiring the spectra between the wavelengths of 4000 cm^{-1} and 375 cm^{-1}, with a resolution of 1.42 cm^{-1}. The absorption peak of amide I **(1703-1605 cm^{-1})** was deconvoluted using OriginPro (version 9.1; OriginLab Corporation, United States) by adapting a protocol previously reported[39]. For the quantification of the samples' crystallinity index (C_i), the different contributions were fit using Gaussian peaks. In the samples with polyurethane and silk blends (BFS, ENC, EtOH and MeOH), the polyurethane contribution was fit together with the silk, with a methodology described in detail in the *Supplementary Information*.

DSC measurements were acquired with a DSC Q200 (TA Instruments; United States) during three heating cycles alternated with periods of cooling and temperature maintenance (see *Supplementary Information*). The second derivative of heat flow during the heating ramp was used to find the glass (T_g), crystallization (T_c) and degradation (T_d) temperatures.

2.5.2 Structure and morphology

The fibrous morphology of samples SF25PU75, SF50PU50, and SF75PU25 was analysed by scanning electron microscopy (SEM). Briefly, each sample was coated with a layer of gold and further observed under a SEM equipment (MIRA3; Tescan, Czech Republic) operating at 10 kV. The diameter of fibres at 5000x magnification was measured using ImageJ software (ImageJ 1.50i; National Institutes of Health, United States) for at least 249 fibres.

2.5.3 Mechanical properties

Uniaxial tensile tests were performed on samples SF25PU75, SF50PU50, and SF75PU25, after cutting dog-bone shaped specimens in the longitudinal direction from opened and flattened electrospun tubular matrices. Tensile properties were measured at RT, after hydrating the samples in distilled water for 10 minutes, using a tensile testing system (LF Plus; Lloyd Instruments, United Kingdom), with a load cell of 100 N, at 100 $mm.min^{-1}$ until break. Strain was calculated in relation to the 24 mm gauge length and stress was calculated in relation to **a cross-sectional area with** 5 mm width and the average thickness measured using a micrometre before starting the test (293-805; Mitutoyo, Japan). Young's modulus was retrieved by doing a linear regression of the elastic domain in each sample. Maximum elongation at break, stress at break and Young's modulus were averaged from 3 replicates and corresponding standard deviations were calculated for each condition. **Dog-bone specimens derived from a commercial ePTFE (expanded polytetrafluoroethylene) graft were similarly tested as a term of comparison (n=2).**

2.5.4 Permeability before and after puncture

Water permeability was measured on samples SF25PU75, SF50PU50, SF75PU25 and on commercial arteriovenous vascular grafts: a polyurethane electrospun graft (ES PU), an ePTFE prosthesis graft, and a three-layered arteriovenous vascular graft containing ePTFE

(3-layer ePTFE). Briefly, a 14 mm diameter circular punch was used to cut samples with consistent size, after longitudinally opening and flattening the electrospun tubular matrices (N≥3 for SF25PU75, SF50PU50, SF75PU25, N=1 for commercial grafts). Each sample was hydrated (demineralised water; t > 10 min) and assembled in a cylindrical chamber held between two silicon O-rings that allowed a circular **perfused** area with a diameter of 11 mm. Each test was conducted at a constant pressure of 120 mmHg for 6 hours. The volume of diffused demineralised water was measured at each hour. The flow rate was further used to calculate the permeability k using Darcy equation (Eq. 1):

$$Q = \frac{k \cdot A \cdot \Delta P}{\mu \cdot L} \qquad \text{(Equation 1)}$$

In Eq. 1, Q is the flow rate, A is the cross-sectional **perfused** area, ΔP is the relative pressure of the medium at the sample location, μ is the viscosity of the medium used, and L is the thickness of the sample.

Following these tests, samples were punctured under 120 mmHg with a 15G haemodialysis needle. The volume of water permeated through the sample was collected for 1 minute, after retrieval of the needle. The measured flow rate was used to calculate the Darcy permeability after puncture.

2.6 Statistical analysis

One-way analysis of variance (ANOVA) was used to perform the statistical analysis where appropriate, considering significance at $P < 0.05$.

3. Results

3.1 Physicochemical properties

Figure 1A shows the full infrared absorbance spectra of samples PP, PFS, FF, FFS, BFS, ENC, EtOH, and MeOH. By comparing sample PP with PFS, and FF with FFS, it is possible to conclude that both polyurethane and fibroin retain their overall characteristic features after dissolution within the proposed solvent system. In fact, the spectrum of PP is comparable to

the PFS aside from a small decrease in absorbance on the two major peaks, at 1740-1735 cm^{-1} (carbonyl, C=O, 1750-1700 cm^{-1}) and 1245-1240 cm^{-1} (ester, –C–O–C–, 1260-1230 cm^{-1}), that could indicate a mild increase in hardness[40]. As to fibroin, typical absorbance bands of amides I (C=O stretching vibration), II (C-N stretching and N-H distortion vibration) and III (C-N stretching and N-H deformation vibration)[27] were observed at peaks 1640, 1514 and 1234 cm^{-1}, respectively, on both FF and FFS, with the latter also retaining all the other nine original peaks (Fig. 1B). However, FFS showed a shift in the amides I, II, and III when compared to sample FF, with the first two shifting towards high wavelengths, and the latter significantly increasing the 1260 cm^{-1} shoulder. This indicates that the used solvent mixture induces a crystallization effect on fibroin, with the development of β-sheet molecular conformations; the effect is observed, as well, when fibroin is blended with polyurethane in sample BFS. Besides that, the analysis of sample BFS confirms that also after blending fibroin and polyurethane maintain their characteristic features, since all peaks detected independently on FFS and PFS were observed in the BFS spectrum, as main peaks or sub-peaks. Interestingly, ENC samples, i.e. electrospun non-crystallized meshes manufactured from the same solution as BFS (cast) samples, did not show a peak shifting in amides I, II, and III as observed in samples FFS and BFS, hinting at the absence of solvent-related crystallization effect upon electrospinning. A possible reason might be the difference in exposure time of fibroin to the solvent mixture, since solvent casting occurred overnight, during several hours, while each electrospinning session (i.e. contact of fibroin with solvents within the solution) took only a couple of hours. Apart from this, the spectrum of ENC was an overlap of FF together with PP or PFS, allowing to conclude that the proposed electrospinning protocol does not induce significant changes in the raw materials. As regards post-processing treatments, EtOH and MeOH spectra were identical, both showing a

crystallization effect in the amide I region in comparison with non-treated electrospun samples (ENC).

Since PP and PFS showed no absorbance on the amide I region, a detailed analysis of the β-sheet contribution was conducted in this region (Fig. 1C, areas highlighted in grey). As shown in the *Supplementary Information*, deconvolution of the absorbance peak of amide I, in all samples, enabled the quantification of the total β-sheet contribution (crystallization index, C_i, Table 2), that resulted 31.4% ± 3.3%, 39.4% ± 2.1%, 37.9% ± 0.5%, 28.4% ± 0.8%, 40.5% ± 0.9%, and 39.6% ± 1.1% for FF, FFS, BFS, ENC, EtOH and MeOH, respectively, confirming the above reported conclusions regarding the crystallization effect of solvents, electrospinning, ethanol and methanol treatments. Further deconvolution analysis revealed that the crystallization effect caused by the solvent mixture (FFS, BFS) was related to the formation of weak β-sheets or aggregated β-strands observed on sub-peaks 1703-1697 cm^{-1} and 1621-1616 cm^{-1}. In fact, inter- and intramolecular strong β-sheets typically observed in two peaks within the 1637-1622 cm^{-1} region[39] were not significant on FFS or BFS versus FF or ENC samples, but were indeed pronounced on samples EtOH and MeOH, revealing a high content of strong β-sheets induced by both crystallization treatments.

Figure 2 represents the heat flow during the heating ramp of DSC performed on samples PP, PFS, FF, FFS, BFS, ENC, EtOH, and MeOH, allowing the extrapolation of the characteristic transitions of each sample (glass transition temperature, T_g, crystallization temperature, T_c, and degradation temperature T_d, summarized in Table 2). Highlighted in grey are the degradation transitions ascribed to fibroin (around 270-300°C) and polyurethane (approximately between 320 and 400°C), which again confirmed the persistence of both materials in blended samples. More in details, the conclusions drawn above as regards the crystallization effect of solvents, electrospinning and post-treatments are corroborated by the

comparison of the crystallization temperatures of FFS (230°C), BFS (226°C), ENC (217°C), EtOH (223°C), and MeOH (227°C) as compared to FF (217°C) samples.

3.2 Structure and morphology

Electrospun hybrid tubular meshes appeared as white hollow cylinders, with an overall length of about 22 cm (Fig. 3A) and inner diameter of approximately 7 mm. SEM images revealed the presence of a fibrous morphology in all samples SF25PU75 (Fig. 3B), SF50PU50 (Fig. 3C) and SF75PU25 (Fig. 3D). There was a reduced presence of beads in SF50PU50 confirming suitable electrospinning parameters for this blend ratio. Diameter analysis revealed a distribution within an overall range of 0.050-2.150 μm. A higher fibre diameter polydispersity was detected on SF25PU75 (Fig. 3E) and SF75PU25 (Fig. 3G) as compared to SF50PU50 (Fig. 3F), which showed a more condensed range of fibre diameter between 0.050-0.800 μm, with an average of 0.316 ± 0.121 μm, confirming optimal fabrication parameters for this formulation. The main morphological characteristics of the electrospun hybrid meshes are summarized in Table 3.

3.3 Mechanical properties

Figure 4 shows the stress-strain plots of the axial tensile tests of SF25PU75 (Fig. 4A), SF50PU50 (Fig. 4B), and SF75PU25 (Fig. 4C) dog-bone specimens. Below, histograms show average values and standard deviations (N=3) of the Young's modulus (Fig. 4D), stress at break (Fig. 4E) and elongation at break (Fig. 4F) of the three blend formulations. A statistically significant increase in Young's modulus is observed in formulations with increasing fibroin content, from 3.96 ± 0.37 MPa for SF25PU75, to 10.60 ± 1.52 MPa for SF50PU50 and 23.50±1.89 MPa for SF75PU25, while an increasing elongation at break is seen in samples with increasing polyurethane content (173 ± 24% for SF25PU75, 127 ± 31% for SF50PU50 and 93 ± 17% for SF75PU25). Interestingly, stress at break revealed no significant difference between different blend ratios, with a mean value of 3.70 ± 0.30 MPa.

Table 3 also summarizes the main mechanical properties of the electrospun hybrid meshes. **ePTFE samples showed an average Young's modulus of 34.66 MPa, elongation at break of 87.77%, and stress at break of 18.73 MPa.**

3.4 Permeability

The Darcy permeability **values** of samples SF25PU75, SF50PU50, and SF75PU25 (Fig. 5) were $2.93\times10^{-17} \pm 1.75\times10^{-17}$ m^2, $9.75\times10^{-18} \pm 1.13\times10^{-18}$ m^2, and $4.19\times10^{-17} \pm 1.26\times10^{-17}$ m^2, respectively (Table 3). These were in the same order of magnitude of commercially available electrospun polyurethane vascular grafts (ES PU), with a permeability of 2.03×10^{-17} m^2. The higher standard deviation in permeability of samples SF25PU75 and SF75PU25 was in line with the frequency in the presence of beads within the same samples, that would require optimization of processing parameters for the corresponding formulations. Samples ePTFE and 3-layer ePTFE were impermeable at 120 mmHg.

3.5 Permeability after puncture

After puncturing the electrospun meshes with a standard haemodialysis needle (15G), the permeability increased by four orders of magnitude in samples SF25PU75, SF50PU50, and SF75PU25 (Fig. 5) to $1.85\times10^{-13} \pm 1.55\times10^{-14}$ m^2, $1.96\times10^{-13} \pm 5.79\times10^{-14}$ m^2, and $1.18\times10^{-13} \pm 2.89\times10^{-14}$ m^2 (Table 3), respectively, following the same trend of the commercially available electrospun vascular grafts, of 8.22×10^{-14} m^2. The gold standard arteriovenous vascular graft composed of an elastomer and ePTFE (3-layer ePTFE), deemed to be capable of self-sealing after puncture, also had permeability of 1.93×10^{-13} m^2. In contrast, the traditional ePTFE graft was completely outperformed, showing a permeability after puncture of 1.10×10^{-12} m^2.

4. Discussion

Despite the increasing interest lately raised by the so-called "*in situ* approach" to tissue engineering[1]–[5], the industrial practicability and the clinical applicability of this strategy, traditionally relying on the use of fully degradable scaffolds, is far from being a reality. The scarcely controllable degradation rate of these scaffolds, which would likely be highly site- and patient-dependent, will make their regulatory approval and clinical transferability, at the very least, complex and adventurous. This is especially true for those applications (e.g. in the cardiovascular district) where a mismatch between the degradation rate of the scaffold and the production of new tissue by the host could dramatically result in the implant's failure, and ultimately in the patient loss. To overcome this limitation, a "hybrid" approach to *in situ* tissue engineering could be adopted, based on the use of semi-degradable scaffolds combining a natural, biodegradable material – typically showing superior bioactivity and biocompatibility - with a synthetic, non-degradable one, granting a permanent backbone with adjustable and stable mechanical properties. This type of scaffold could be particularly beneficial in the field of vascular accesses (i.e. the arteriovenous shunts that allow for haemodialysis), where there is an urgent, unmet, global need for grafts that show suitable mechanical properties for early cannulation (i.e. that can be punctured immediately after implantation), as well as the capability to integrate and remodel in the long-term, which is known to be the key to a positive clinical outcome[6].

Based on this rationale, in this work we report the successful blending of regenerated silk fibroin with an aromatic**, medical grade, highly biocompatible** poly-carbonate-urethane[38] by using a solvent mixture of formic acid and dichloromethane, and the manufacture of electrospun hybrid tubular meshes, whose properties can be tuned according to the respective ratios of the raw materials in the blend. Indeed, our approach overcomes the limitations of several studies, already cited in the introductory section in this work, coupling fibroin and polyurethane in an attempt at combining the properties of natural and synthetic materials. In

particular, making use of solvents addressed by the European Pharmacopeia[35], and blending fibroin together with a non-degradable polyurethane, we offer a potential industrially-sustainable solution to regulatory hurdles (related to residual solvents and degradable polyurethanes) and technical issues (the separation of fibroin and polyurethane during processing).

In our study, fibroin and polyurethane were processed through several steps, namely: dissolution, blending, electrospinning and post-treatment, which could have altered the materials' intrinsic properties. The first part of the work, therefore, was dedicated to the investigation of the effects of each processing step on the raw materials (used in a 1:1 ratio in the blend formulations, Table 1).

Physicochemical analyses (Fig. 1, Fig. 2, Table 2) demonstrated that both materials retained their characteristic features after dissolution within the proposed solvent system, and allowed to rule out possible denaturation, degradation, or chemical reactions between them in the blend; also, electrospun blend samples did not show significant effects on the raw materials if compared with cast blend films. Peculiar attention was dedicated to the analysis of the effect of the different processing steps on the crystallization of fibroin. **The degree of crystallinity of silk fibroin, which is related to its molecular conformations (fraction of β-sheets in relation to α-helix and random turns[39]), is in fact known to significantly affect the material's characteristics, e.g. in terms of solubility, mechanical properties, and degradation rate[41]. Indeed, regenerated fibroin can be water soluble and mechanically unstable in the amorphous state (higher α-helix fraction) or insoluble and mechanically stable in the crystalline state (predominant β-sheet fraction)[42],[43]. In the perspective, pursued in this work, of an industrially sustainable scaffold manufacturing process, the characterization, and possibly the control of the degree of crystallization of fibroin, is imperative to ensure reproducibility of the process and repeatability of the**

product's features (e.g., shelf life, *in vivo* degradation rate, stiffness). To this purpose, deconvolution of the amide I peak allowed to calculate the crystallization index (C_i) of fibroin-containing samples. As regards the post-processing treatments, we demonstrated that the proposed ethanol-based protocol induces a similar crystallization effect as compared to the traditional methanol-based one (more expensive and hazardous). Interestingly, both EtOH and MeOH samples revealed a higher glass transition temperature of 202ºC as compared to the 181.3-182.6ºC recorded in all other samples. Hu *et al.* also analysed fibroin samples crystallized with methanol, by DSC, and likewise observed a glass transition temperature of 202 ºC, indicating that this effect is caused by β-sheet crystallization[39]. However, the same was not observed in samples FFS an BFS, where the glass transition temperature remained equal to FF samples, but both the crystallization temperature and index were in line with EtOH and MeOH samples. Deconvolution of the FTIR absorbance of amide I peak, in all samples, revealed that the crystallization effect caused by the overnight exposure to the solvent mixture (FFS, BFS) was related to the formation of weak β-sheets or aggregated β-strands observed on sub-peaks 1703-1697 cm^{-1} and 1621-1616 cm^{-1}. In fact, inter- and intramolecular strong β-sheets typically observed in two peaks at the 1637-1622 cm^{-1} region[39] were not significant on FFS or BFS versus FF samples, but were indeed pronounced on samples EtOH and MeOH, revealing a high content of strong β-sheets induced by both crystallization treatments. Upon observing that the effects of ethanol and methanol produced the same type and degree of crystallization, the average spectrum of EtOH samples was subtracted from the MeOH average, to evaluate what remained (see *Supplementary Information*): interestingly, three major peaks were observed at 1740-1720 cm^{-1} and 1260-1230 cm^{-1}, which coincide with characteristic peaks of formic acid and dichloromethane[44]. Although the typical peaks of polyurethane and fibroin fall in these regions, not allowing a trustworthy quantitative analysis by deconvolution, this result – not

surprisingly - indicates that the additional washing steps and time associated to the ethanol post-processing treatment were also more effective in removing residual solvents than the simple soaking in methanol. **As regards the solvents used in this study, it is worth noticing that, while formic acid is included in Class 3 (Solvents with low toxic potential) by the European Pharmacopoeia[35], dichloromethane belongs to Class 2 (Solvents to be limited), with a maximum concentration allowed of 600 ppm. Indeed, more refined analyses (e.g. thermogravimetric analysis, TGA) will need to be performed on the final product (i.e., after sterilization) to ensure a quantification of solvent residuals within the mesh; however, it has to be considered that additional post-processing steps, potentially effective in removing residual solvents, can still be explored, e.g. vacuum drying.**

After assessing the dissolution, blending, electrospinning and post-treatment techniques, our study focused on the evaluation of the applicability of the proposed process to blends with different respective ratios of fibroin and polyurethane. To this purpose, hybrid tubular meshes were electrospun using solutions with 1:3 (SF25PU75), 1:1 (SF50PU50), 3:1 (SF25PU75) ratios of fibroin and polyurethane. The meshes were characterized in terms of morphology, and, envisioning their possible use as substrates for vascular grafts, the mechanical properties and permeability were also evaluated.

SEM micrographs revealed a fibrous morphology mostly at the sub-micrometric level, with virtually indistinguishable, intermingled fibroin/polyurethane fibres (Fig. 3). The fact that fibroin and polyurethane respond to electrospinning and post-processing treatments without undergoing separation and/or delamination, as elsewhere reported for composite/coated scaffolds[30], reassures about the robustness of the proposed technique and suggests that the material could show potential for a gradual *in situ* remodelling of the fibroin portion of the scaffold, with the polyurethane backbone being incorporated into the newly-formed tissue, sustaining the mechanical properties of the overall implant.

Such a stable coalescence between fibroin and polyurethane in all the formulations was confirmed by the uniaxial tensile behaviour of the electrospun samples (Fig. 4), which showed a neat and sharp profile, with no signs of the saw-toothed morphology typical of delaminating structures. Not surprisingly, mechanical tests also confirmed that increasing the fibroin content in the blend significantly increases the stiffness of the mesh, whereas increasing the polyurethane content in the blend determines an increase in the elongation at break (Table 3); this fact shows the possibility of tuning of the mechanical properties of the scaffold to the ones in the implant site, which is known to be a crucial factor especially in the vascular field, where **graft-vessel compliance mismatch is recognized as one of the major determinants of grafts' failures**[45]. Indeed, samples SF25PU75 and SF50PU50 demonstrated a Young's modulus in line with the values reported in the literature for peripheral arteries, i.e. 1-10 MPa, such as the radial and brachial arteries[46]–[48]. **In contrast, our tests revealed that ePTFE has a Young's modulus around 35 MPa; although the literature is inconsistent in reporting the mechanical properties of ePTFE (Young's modulus of tens of MPa**[49] **to few GPa**[50]**), possibly due to different types of grafts under study, a clear divergence in mechanical properties is observed when compared with peripheral arteries.** Also, no significant difference between the formulations was observed in terms of stress at break, possibly confirming that fibroin and polyurethane are perfectly coalescent within the mesh, and both contribute as load-bearing structures.

Permeability tests (Fig. 5) allowed to verify that the electrospun meshes are characterized by k values (Darcy permeability) in the same order of magnitude ($k \approx 10^{-17}$ **m^2**) as commercially available electrospun polyurethane grafts already used in the clinics (ES PU), hinting at their possibly favourable *in situ* behaviour in terms of avoidance of seroma formation. The measurements also confirmed that ePTFE-containing grafts, known to suffer from scarce integration with the host tissue, are in fact impermeable at 120 mmHg. Finally,

the evaluation of permeability after puncture with a dialysis needle (15G) showed that the behaviour of the electrospun meshes is strikingly similar ($k \approx 10^{-13}$ **m²**) to the one of commercial grafts that are deemed to be suitable for early cannulation (ES PU and 3-layer ePTFE), i.e. capable of self-sealing after puncture and avoiding massive bleeding at the puncture site.

In summary, herein we proposed a novel blending technique for fibroin and polyurethane, using industrially-sustainable solvents (affordable, moderately volatile, addressed by the European Pharmacopoeia), regenerated fibroin and a medical-grade poly-carbonate-urethane suitable for long-term implantation, which proved to be effective in maintaining the characteristic physicochemical features of the two materials. We also demonstrated the feasibility of electrospinning blend solutions with varying ratios of fibroin and polyurethane, to obtain hybrid tubular meshes possessing extracellular matrix-*like* nano-fibrous morphology, tuneable mechanical properties, and favourable permeability before and after puncture, therefore representing possible substrates for semi-degradable haemodialysis vascular accesses.

Future work will focus on further optimization of the architectural structure of a novel arteriovenous graft for haemodialysis, whose performances will be characterized *in vitro* and *in vivo*, in view of an alternative, "hybrid" approach to *in situ* vascular tissue engineering.

Acknowledgements

This work was supported by the European Commission within the Horizon 2020 Framework through the MSCA-ITN-ETN European Training Networks (project number 642458). The authors would like to acknowledge the Medical Doctors Franco Galli, Luciano Carbonari and Matteo Tozzi for providing inspiration for the development of this work.

Conflicts of interest

Sebastião van Uden and Stefania A. Riboldi are employees of Bioengineering Laboratories S.r.l., and Francesco G. Greco is President and Chief Executive Officer of Bioengineering Laboratories S.r.l..

References

1. Kluin J, Talacua H, Smits AIPM, Emmert MY, Brugmans MCP, Fioretta ES, Dijkman PE, Söntjens SHM, Duijvelshoff R, Dekker S, Janssen-van den Broek MWJT, Lintas V, Vink A, Hoerstrup SP, Janssen HM, Dankers PYW, Baaijens FPT, Bouten CVC. In situ heart valve tissue engineering using a bioresorbable elastomeric implant - From material design to 12 months follow-up in sheep. Biomaterials. 2017;125:101–17.

2. Talacua H, Smits AIPM, Muylaert DEP, van Rijswijk JW, Vink A, Verhaar MC, Driessen-Mol A, van Herwerden LA, Bouten CVC, Kluin J, Baaijens FPT. In Situ Tissue Engineering of Functional Small-Diameter Blood Vessels by Host Circulating Cells Only. Tissue Eng Part A. 2015;21:2583–94.

3. Cattaneo I, Figliuzzi M, Azzollini N, Catto V, Farè S, Tanzi MC, Alessandrino A, Freddi G, Remuzzi A. In vivo regeneration of elastic lamina on fibroin biodegradable vascular scaffold. Int J Artif Organs. 2013;36:166–74.

4. Matsumura G, Nitta N, Matsuda S, Sakamoto Y, Isayama N, Yamazaki K, Ikada Y. Long-Term Results of Cell-Free Biodegradable Scaffolds for In Situ Tissue-Engineering Vasculature: In a Canine Inferior Vena Cava Model. PLoS One. 2012;7:e35760.

5. Rothuizen TC, Damanik FFR, Lavrijsen T, Visser MJT, Hamming JF, Lalai RA, Duijs JMGJ, van Zonneveld AJ, Hoefer IE, van Blitterswijk CA, Rabelink TJ, Moroni L, Rotmans JI. Development and evaluation of in vivo tissue engineered blood vessels in a porcine model. Biomaterials. 2016;75:82–90.

6. Peck MK, Dusserre N, Zagalski K, Garrido S a., Wystrychowski W, Glickman MH, Chronos N a. F, Cierpka L, L'Heureux N, McAllister TN. New biological solutions for hemodialysis access. J Vasc Access. 2011;12:185–92.

7. https://www.accessdata.fda.gov/scripts/cdrh/cfdocs/cfcfr/CFRSearch.cfm?fr=878.5030. US Food and Drug Administration. 2017.

8. Santin M, Motta A, Freddi G, Cannas M. In vitro evaluation of the inflammatory potential of the silk fibroin. J Biomed Mater Res. 1999;46:382–9.

9. Meinel L, Hofmann S, Karageorgiou V, Kirker-Head C, McCool J, Gronowicz G, Zichner L, Langer R, Vunjak-Novakovic G, Kaplan DL. The inflammatory responses to silk films in vitro and in vivo. Biomaterials. 2005;26:147–55.

10. Gholipourmalekabadi M, Mozafari M, Bandehpour M, Salehi M, Sameni M, Caicedo HH, Mehdipour A, Hamidabadi HG, Samadikuchaksaraei A, Ghanbarian H. Optimization of nanofibrous silk fibroin scaffold as a delivery system for bone marrow adherent cells: in vitro and in vivo studies. Biotechnol Appl Biochem. 2015;62:785–94.

11. Sakabe H, Ito H, Miyamoto T, Noishiki Y, Ha WS. In vivo blood compatibility of regenerated silk fibroin. Sen'i Gakkaishi. 1989;45:487–90.

12. Zhang J, Huang H, Ju R, Chen K, Li S, Wang W, Yan Y. In vivo biocompatibility and hemocompatibility of a polytetrafluoroethylene small diameter vascular graft modified with sulfonated silk fibroin. Am J Surg. 2017;213:87–93.

13. Marois Y, Guidoin R. Biocompatibility of Polyurethanes. In: Madame Curie Bioscience Database. Austin (TX): Landes Bioscience; 2000–2013.

14. Hu J, Chen B, Guo F, Du J, Gu P, Lin X, Yang W, Zhang H, Lu M, Huang Y, Xu G. Injectable silk fibroin/polyurethane composite hydrogel for nucleus pulposus replacement. J Mater Sci Mater Med. 2012;23:711–22.

15. Cai L, Han F, Hu J, Xu G, Huang Y, Lin X. The effect of the preparation process on the swelling behavior of silk fibroin-polyurethane composite hydrogels using a full factorial experimental design. J Polym Eng. 2015;35:523–31.

16. Suzuki Y, Nakazawa Y, Derya A, Komatsu T, Miyazaki K, Yamazaki S, Asakura T. Development of silk/polyurethane small-diameter vascular graft by electrospinning. Seikei-Kakou. 2013;25:181–7.

17. Yu E, Zhang J, Thomson JA, Turng L-S. Fabrication and Characterization of Electrospun Thermoplastic Polyurethane/Fibroin Small-Diameter Vascular Grafts for Vascular Tissue Engineering. Int Polym Process. 2016;31:638–46.

18. Park H, Gong M-S, Park J-H, Moon S, Wall IB, Kim H-W, Lee JH, Knowles JC. Silk fibroin–polyurethane blends: Physical properties and effect of silk fibroin content on viscoelasticity, biocompatibility and myoblast differentiation. Acta Biomater. 2013;9:8962–71.

19. Shimada K, Higuchi A, Kubo R, Murakami T, Nakazawa Y, Tanaka R. The effect of a silk Fibroin/Polyurethane blend patch on rat Vessels. Organogenesis. 2017;0:1–10.

20. Nakazawa CT, Higuchi A, Asano A, Kameda T, Aytemiz D, Nakazawa Y. Solid-state NMR studies for the development of non-woven biomaterials based on silk fibroin and polyurethane. Polym J. 2017;49:583–6.

21. Zhou M, Wang W-C, Liao Y-G, Liu W-Q, Yu M, Ouyang C-X. In vitro biocompatibility evaluation of silk-fibroin/polyurethane membrane with cultivation of

HUVECs. Front Mater Sci. 2014;8:63–71.

22. Yang H-J, Xu H-Y, Zhu G-C, Ouyang C-X, Wang X-G, Xu W-L. Composite membranes of native silk fibroin powder and biomedical polyurethane for controlled release of heparin. Proc Inst Mech Eng Part H J Eng Med. 2011;225:421–33.

23. Liu X, Zhang C, Xu W, Liu H, Ouyang C. Blend films of silk fibroin and water-insoluble polyurethane prepared from an ionic liquid. Mater Lett. 2011;65:2489–91.

24. Liu X-Y, Zhang C-C, Xu W-L, Ouyang C. Controlled release of heparin from blended polyurethane and silk fibroin film. Mater Lett. 2009;63:263–5.

25. Um IC, Kweon HY, Hwang CM, Min B-G, Park Y-H. Structural characteristics and properties of silk fibroin/polyurethane blend films. Int J Ind Entomol. 2002;5:163–70.

26. Liu H, Xu W, Zou H, Ke G, Li W, Ouyang C. Feasibility of wet spinning of silk-inspired polyurethane elastic biofiber. Mater Lett. 2008;62:1949–52.

27. Bai Z, Xu W, Xu J, Yang H, Xiao S, Liu X, Liang G, Chen L. Fabrication and Characterization of Silk Fibroin Powder/Polyurethane Fibrous Membrane. Polym Eng Sci. 2012;52:2025–32.

28. Tao Y, Yan Y, Xu W, Zhou W. Preparation, structure and properties of blended films of polyurethane and silk fibroin. Acta Polym Sin. 2010;10:27–32.

29. dal Prà I, Petrini P, Charini A, Bozzini S, Farè S, Armato U. Silk Fibroin-Coated Three-Dimensional Polyurethane Scaffolds for Tissue Engineering: Interactions with Normal Human Fibroblasts. Tissue Eng. 2003;9:1113–21.

30. Petrini P, Chiarini A, Bozzini S, dal Prà I, Farè S, Armato U. Silk fibroin-polyurethane scaffolds for tissue engineering. J Mater Sci Mater Med. IEEE; 2001;12:849–53.

31. Chiarini A, Petrini P, Bozzini S, Prà I dal, Armato U. Silk fibroin/poly(carbonate)-urethane as a substrate for cell growth: in vitro interactions with human cells. Biomaterials. 2002;24:789–99.

32. Li JF, Chen ZM, Luo Q, Zhang GH, Wang FP. Preparation and Biological Properties of Nano-Silk Fibroin/Polyurethane/Silver Nanoparticles Composite Membranes. Mater Sci Forum. 2016;848:557–66.

33. Luo Z, Zhang Y, Zhou H, Liao J, Zhang X, Wu Q. A one-pot preparation of silk fibroin modified with polyurethane micro-particles. New J Chem. 2013;37:3109.

34. Iizuka E, Sawada K, Motojima K. Physical properties of fibroin-blended polyurethane films. J Sericultural Sci Japan. 1998;67:217–21.

35. European Pharmacopoeia. 8th ed. European Directorate for the Quality of Medicines - Council of Europe; 2014.

36. Tanzi MC, Ambrosio L, Nicolais L, Iannace S, Ghislanzoni L, Mambrito B. Comparative physical tests on segmented polyurethanes for cardiovascular applications. Clin Mater. 1991;8:57–64.

37. Cheng Y-H, Yang S-H, Lin F-H. Thermosensitive chitosan-gelatin-glycerol phosphate hydrogel as a controlled release system of ferulic acid for nucleus pulposus regeneration. Biomaterials. 2011;32:6953–61.

38. https://www.lubrizol.com/-/media/Lubrizol/Life-Sciences/Documents/TDS/Carbothane-TPU-Clear-Aromatic.pdf. Lubrizol Advanced Materials, Inc. Cleveland, Ohio USA; 2016.

39. Hu X, Kaplan D, Cebe P. Determining Beta-Sheet Crystallinity in Fibrous Proteins by Thermal Analysis and Infrared Spectroscopy. Macromolecules. 2006;39:6161–70.

40. Park S-H, Gil ES, Mandal BB, Cho H, Kluge JA, Min B-H, Kaplan DL. Annulus fibrosus tissue engineering using lamellar silk scaffolds. J Tissue Eng Regen Med. 2012;6:s24–33.

41. Pignatelli C, Perotto G, Nardini M, Cancedda R, Mastrogiacomo M, Athanassiou A. Electrospun silk fibroin fibers for storage and controlled release of human platelet lysate. Acta Biomater. 2018.

42. Hu X, Shmelev K, Sun L, Gil ES, Park SH, Cebe P, Kaplan DL. Regulation of silk material structure by temperature-controlled water vapor annealing. Biomacromolecules. 2011;12:1686–96.

43. Vepari C, Kaplan DL. Silk as a biomaterial. Prog Polym Sci. 2007;32:991–1007.

44. Linstrom PJ, Mallard WG, editors. NIST Chemistry webBook, NIST Standard Reference Database Number 69. Gaithersburg MD: National Institute of Standards and Technology; 2017.

45. Li L, Terry CM, Shiu YE, Cheung AK. Neointimal hyperplasia associated with synthetic hemodialysis grafts. Kidney Int. 2008;74:1247–61.

46. Mourad J-J, Girerd X, Boutouyrie P, Laurent S, Safar M, London G. Increased Stiffness of Radial Artery Wall Material in End-Stage Renal Disease. Hypertension. 1997;30:1425–30.

47. Bank AJ, Kaiser DR, Rajala S, Cheng A. In Vivo Human Brachial Artery Elastic Mechanics : Effects of Smooth Muscle Relaxation. Circulation. 1999;100:41–7.

48. Laurent S, Girerd X, Mourad JJ, Lacolley P, Beck L, Boutouyrie P, Mignot JP, Safar M. Elastic modulus of the radial artery wall material is not increased in patients with essential hypertension. Arterioscler Thromb a J Vasc Biol. 1994;14:1223–31.

49. Paasche PE, Kinley CE, Dolan FG, Gozna ER, Marble AE. Consideration of suture line stresses in the selection of synthetic grafts for implantation. J Biomech. 1973;6:253–9.

50. Jørgensen CS, Paaske WP. Physical and mechanical properties of ePTFE stretch vascular grafts determined by time-resolved scanning acoustic microscopy. Eur J Vasc Endovasc Surg. 1998;15:416–22.

Figure captions

Figure 1. FTIR spectra of samples PP, PFS, FF, FFS, BFS, ENC, EtOH, and MeOH, (A) at full scale, (B) between 1800-1100 cm^{-1} and (C) at the amide I region. Dashed lines represent the characteristic wavelengths of polyurethane (at 1740-1735 cm^{-1} and 1245-1240 cm^{-1}) and fibroin (amides I, II and III around 1640, 1514 and 1234 cm^{-1}). Regions highlighted in grey allow to detect the crystallization effect of solvents (FFS and BFS vs FF), electrospinning (ENC vs BFS), ethanol- and methanol-treatments (EtOH and MeOH vs ENC) on fibroin β-sheet arrangements.

Figure 2. DSC analysis plots of samples PP, PFS, FF, FFS, BFS, ENC, EtOH, and MeOH, showing the final heating phase. Highlighted in grey are the degradation transitions ascribed to fibroin (around 270-300°C) and polyurethane (approximately between 320 and 400°C).

Figure 3. Structure and morphology of tubular electrospun hybrid meshes composed by a blend of fibroin and polyurethane. (A) Macroscopic appearance of an exemplifying SF50PU50 sample. SEM micrographs of samples SF25PU75 (B), SF50PU50 (C), and SF75PU25 (D), with a 10 μm scale bar. Histograms presenting the fibre diameter analysis of samples SF25PU75 (E), SF50PU50 (F), and SF75PU25 (G).

Figure 4. Stress-strain plots of uniaxial tensile tests performed on samples SF25PU75 (A), SF50PU50 (B), and SF75PU25 (C), allowing for the calculation of Young's modulus (D), stress at break (E) and elongation at break (F). Results are expressed as average ± standard deviation, n=3. *: significance was considered at $P<0.05$.

Figure 5. Darcy permeability (k) of samples SF25PU75, SF50PU50, and SF75PU25, as compared to commercially available grafts (ES PU=polyurethane electrospun graft, ePTFE=expanded polytetrafluoroethylene graft, 3-layer ePTFE=three-layered graft containing ePTFE), before (white columns) and after (criss-cross columns) puncturing with a needle (15G) typically used in haemodialysis procedure (N≥3 for SF25PU75, SF50PU50,

SF75PU25, N=1 for commercial grafts). ES PU and 3-layer ePTFE are deemed to be grafts capable of self-sealing after retrieval of the needle (i.e. low permeability after puncture).

Table 1. Processing parameters used to prepare samples PP, PFS, FF, FFS, BFS, ENC, EtOH and MeOH, regarding concentration of raw materials and organic solvents used on solution preparation, electrospinning parameters and post-treatment times employed. SF=silk fibroin, PU=polyurethane, FA=formic acid, DCM=dichloromethane, t=processing time, ΔV=electrospinning voltage, d=distance between spinneret and collector, Q=flow rate of electrospinning solution, EtOH*=ethanol-based post-treatment, MeOH*=methanol-based post-treatment.

Sample acronym	Sample long name	%SF [w/v]	%PU [w/v]	FA:DCM [v:v]	t [h]	ΔV [kV]	d [cm]	Q [ml/h]	EtOH* [hh:mm]	MeOH* [hh:mm]
PP	Polyurethane pellets	-	100%	-	-	-	-	-	-	-
PFS	Solvent cast polyurethane films	-	2%	3:2	O/N	-	-	-	-	-
FF	Aqueous fibroin films	100%	-	-	-	-	-	-	-	-
FFS	Solvent cast fibroin films	2%	-	3:2	O/N	-	-	-	-	-
BFS	Solvent cast blend films	2%	2%	3:2	O/N	-	-	-	-	-
ENC	Electrospun hybrid mesh non-crystallized	2%	2%	3:2	8h	17	19	2.5	-	-
EtOH	Electrospun hybrid mesh crystallized with ethanol	2%	2%	3:2	8h	17	19	2.5	20:00	-
MeOH	Electrospun hybrid mesh crystallized with methanol	2%	2%	3:2	8h	17	19	2.5	-	00:10

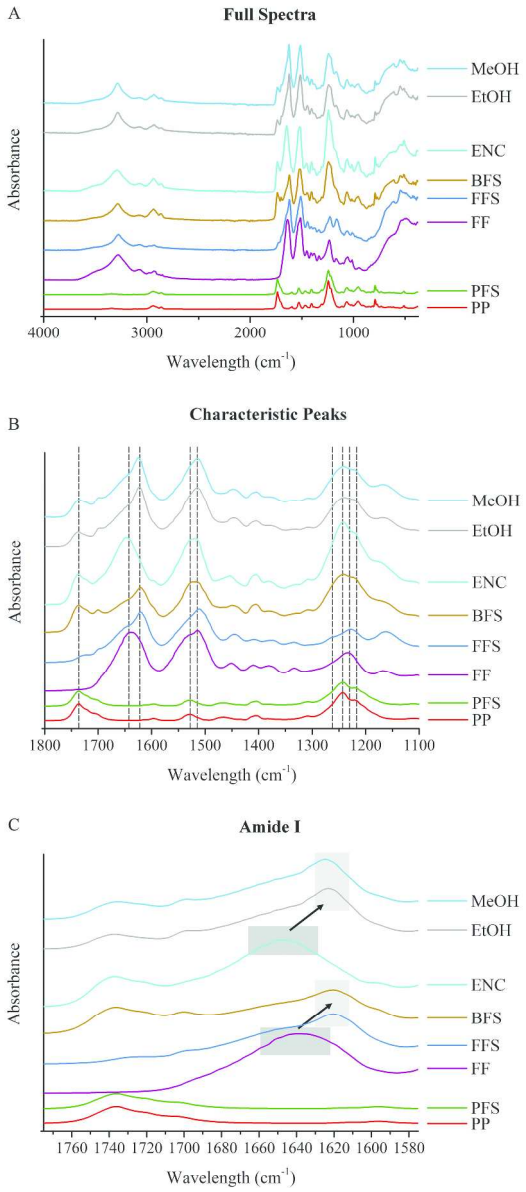

Figure 1. FTIR spectra of samples PP, PFS, FF, FFS, BFS, ENC, EtOH, and MeOH, (A) at full scale, (B) between 1800-1100 cm^{-1} and (C) at the amide I region. Dashed lines represent the characteristic wavelengths of polyurethane (at 1735-1740 cm^{-1} and 1240-1245 cm^{-1}) and fibroin (amides I, II and III around 1640, 1514 and 1234 cm^{-1}). Regions highlighted in grey allow to detect the crystallization effect of solvents (FFS and BFS vs FF), electrospinning (ENC vs BFS), ethanol- and methanol-treatments (EtOH and MeOH vs ENC) on fibroin β-sheet arrangements.

195x418mm (600 x 600 DPI)

Table 2. Physicochemical analysis of samples PP, PFS, FF, FFS, BFS, ENC, EtOH and MeOH: crystallization index (C_i), glass (T_g), crystallization (T_c) and degradation (T_d) temperatures. Degradation temperatures ascribed to fibroin (1°) and polyurethane (2°) are shown separately for samples containing both materials (BFS, ENC, EtOH, MeOH).

	C_i	T_g	T_c	T_d
FF	31.4% ± 3.3%	181.3	217	292
FFS	39.4% ± 2.1%	182.6	230	287
PP	-	-	-	369
PFS	-	-	-	354
BFS	37.9% ± 0.5%	182.6	226	1° - 293 2° - 358
ENC	28.4% ± 0.8%	182.6	217	1° - 295 2° - 357
EtOH	40.5% ± 0.9%	202	223	1° - 294 2° - 324
MeOH	39.6% ± 1.1%	202	227	1° - 295 2° - 339

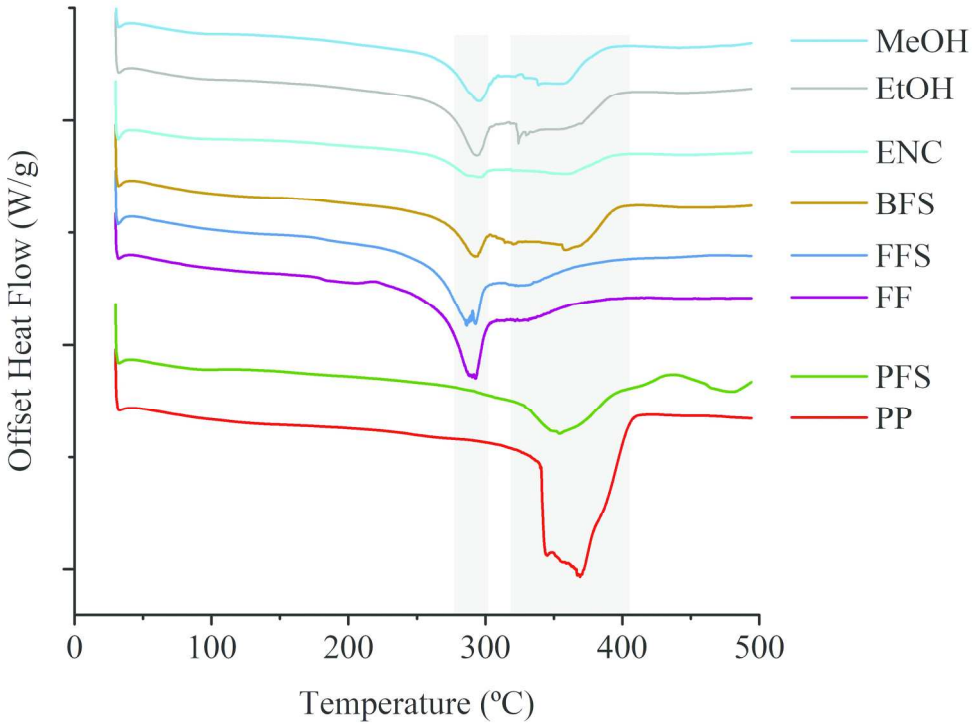

Figure 2. DSC analysis plots of samples PP, PFS, FF, FFS, BFS, ENC, EtOH, and MeOH, showing the final heating phase. Highlighted in grey are the degradation transitions ascribed to fibroin (around 270-300°C) and polyurethane (approximately between 320 and 400°C).

114x83mm (600 x 600 DPI)

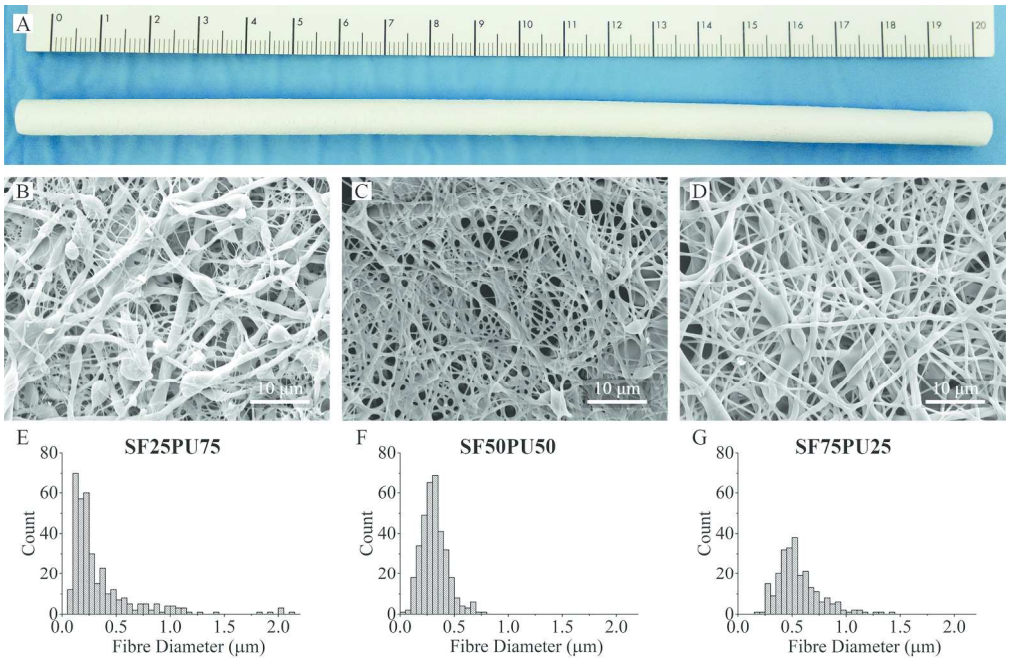

Figure 3. Structure and morphology of tubular electrospun hybrid meshes composed by a blend of fibroin and polyurethane. (A) Macroscopic appearance of an exemplifying SF50PU50 sample. SEM micrographs of samples SF25PU75 (B), SF50PU50 (C), and SF75PU25 (D), with a 10 µm scale bar. Histograms presenting the fibre diameter analysis of samples SF25PU75 (E), SF50PU50 (F), and SF75PU25 (G).

108x71mm (600 x 600 DPI)

Table 3. Quantitative characteristics of all formulations of electrospun hybrid meshes: SF25PU75, SF50PU50 and SF75PU25, regarding wall thickness, fibre diameter, mechanical properties, and permeability (k) before and after puncture.

	SF25PU75	SF50PU50	SF75PU25
Wall thickness (mm)	130± 26	164±22	182±21
$\varnothing_{fibre}$ (mm)	0.348±0.329	0.316±0.121	0.559±0.203
E (MPa)	3.96±0.37	10.60±1.52	23.50±1.89
Elongation at break (%)	173±24	127±31	93±17
Stress at break (MPa)	3.65±0.13	3.35±0.58	4.09±0.44
k (m^2) before puncture	$2.93\times10^{-17}\pm1.75\times10^{-17}$	$9.75\times10^{-18}\pm1.13\times10^{-18}$	$4.19\times10^{-17}\pm1.26\times10^{-17}$
k (m^2) after puncture	$1.85\times10^{-13}\pm1.55\times10^{-14}$	$1.96\times10^{-13}\pm5.79\times10^{-14}$	$1.18\times10^{-13}\pm2.89\times10^{-14}$

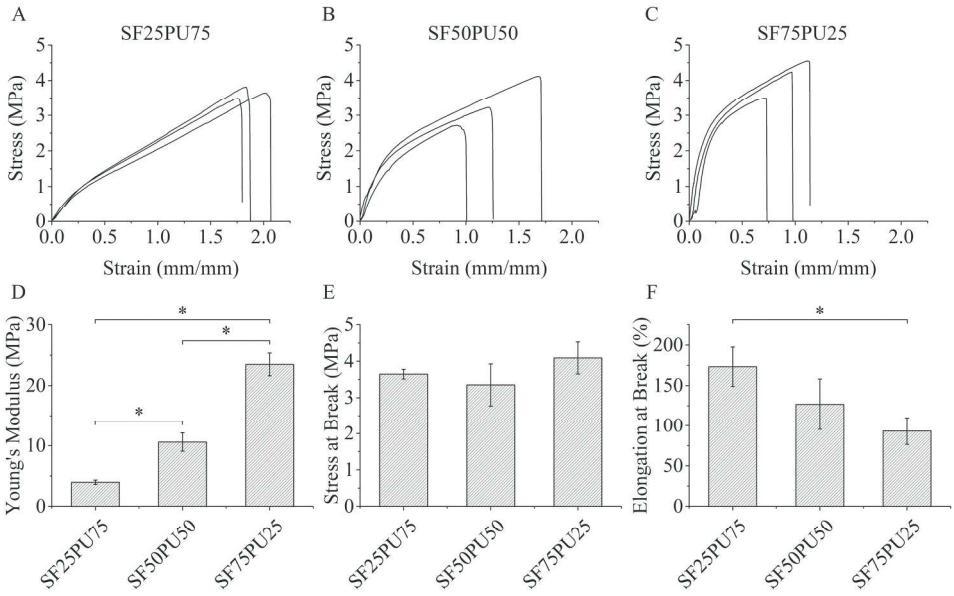

Figure 4. Stress-strain plots of uniaxial tensile tests performed on samples SF25PU75 (A), SF50PU50 (B), and SF75PU25 (C), allowing for the calculation of Young's modulus (D), stress at break (E) and elongation at break (F). Results are expressed as average ± standard deviation, n=3. *: significance was considered at P<0.05.

107x68mm (600 x 600 DPI)

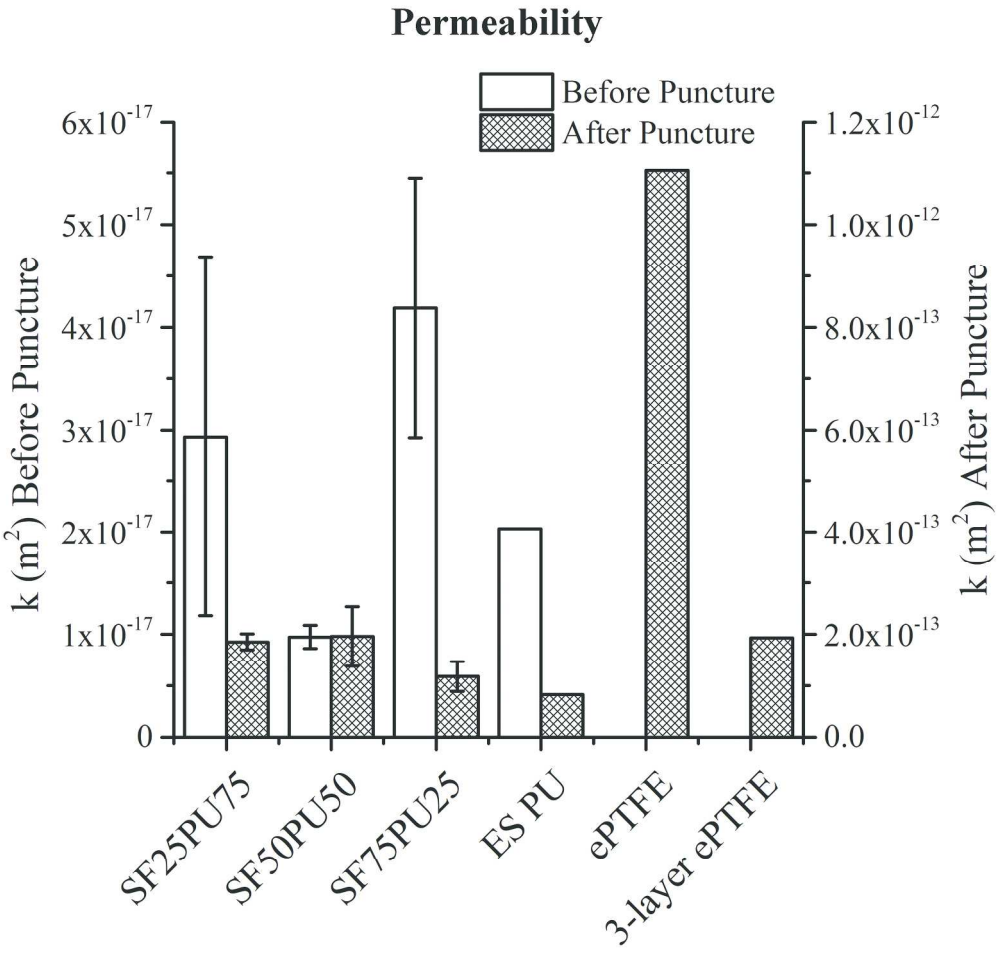

Figure 5. Darcy permeability (k) of samples SF25PU75, SF50PU50, and SF75PU25, as compared to commercially available grafts (ES PU=polyurethane electrospun graft, ePTFE=expanded polytetrafluoroethylene graft, 3-layer ePTFE=three-layered graft containing ePTFE), before (white columns) and after (criss-cross columns) puncturing with a needle (15G) typically used in haemodialysis procedure (N≥3 for SF25PU75, SF50PU50, SF75PU25, N=1 for commercial grafts). ES PU and 3-layer ePTFE are deemed to be grafts capable of self-sealing after retrieval of the needle (i.e. low permeability after puncture).

132x130mm (600 x 600 DPI)